Elektrocatalysis

DOI: 10.1002/ange.201307305

A Highly Active Perovskite Electrode for the Oxygen Reduction Reaction Below 600 °C**

Wei Zhou, Jaka Sunarso, Mingwen Zhao, Fengli Liang, Tobias Klande, and Armin Feldhoff**

A low-temperature solid oxide fuel cell (SOFC) is an attractive new concept, uniquely combining the advantages of relatively low-temperature operation ($\leq 600\,^{\circ}C$) and fuel flexibility.[1–4] Central to this device is the availability of a highly active oxygen reduction reaction (ORR) catalyst.[5–8] If the operating temperature of the SOFC can be lowered to below 600 °C, it would be more competitive against hydrogen-fuelled polymer electrolyte membrane fuel cells, which operate below 200 °C, in terms of reduced system and operation costs, higher theoretical fuel efficiency at decreasing temperature, larger volumetric and gravimetric power densities and similar specific energy (based on liquid hydrocarbons) of SOFCs relative to internal combustion engines.[5,6]

Addressing the polarization losses of the SOFC components (e.g., cathode, electrolyte, and anode) at these low temperatures has been the main challenge. For the electrolyte and anode, for example, anode-supported electrolyte, major advances have been demonstrated by fabricating metallic grids supporting a nanometer-thin electrolyte layer[9] and adopting a highly conductive electrolyte consisting of functionally graded bi-layer materials (e.g., Gd-doped CeO_2/Er-doped Bi_2O_3 and Sm-Nd-doped CeO_2/Dy-W-doped Bi_2O_3).[10,11] Therefore, the oxygen reduction reaction (ORR) at the cathode side, rather than ionic conduction in the electrolyte and fuel oxidation at the anode side, is currently limiting the SOFC performance below 600 °C.[12,13] This is reflected in most cathodes by high activation energy for ORR (e.g., thermally activated), which leads to substantial degradation in the ORR properties upon changing the temperature, as well as a relatively high enthalpy of ionic motion, which limits the ORR onset temperature to a high range.[14,15]

There has been an ongoing search over the last two decades for a highly active cathode. One of the milestones was a cathode based on mixed ionic–electronic conducting oxides (e.g., oxides featuring simultaneous oxygen-ion and electron transport capabilities).[16,17] A reasonably high ORR performance at 600 °C is afforded by their high ionic and electronic conductivity, which allows the ORR to be extended from the three-phase boundary (for the nonmixed ionic–electronic conductors, or non-MIEC) to the overall surface area of MIEC cathodes.[18] Several cathode compositions, for example, $Sm_{0.5}Sr_{0.5}CoO_{3-\delta}$, $Ba_{0.5}Sr_{0.5}Co_{0.8}Fe_{0.2}O_{3-\delta}$ (BSCF), $SrSc_{0.2}Co_{0.8}O_{3-\delta}$, and $SrNb_{0.1}Co_{0.9}O_{3-\delta}$, all from the perovskite family, have since been reported that show promising ORR activity at and above 600 °C.[19–22]

Herein, we report a novel perovskite composition, $SrSc_{0.175}Nb_{0.025}Co_{0.8}O_{3-\delta}$ (SSNC), which shows a rapid bulk oxygen diffusion rate below 550 °C, enabling the oxygen reduction reactivity on an SSNC electrode to be enhanced by 100 % at 500 °C relative to the prominent cathode material, BSCF. We also demonstrate, through first-principles calculations, the existence of two oxygen ion transport paths with very low migration barrier energies created upon partially substituting Co atoms into the $SrCoO_{3-\delta}$ lattice with Nb and Sc atoms as the origin to this extremely high activity. SSNC, incorporated into samarium-doped ceria (SDC) fuel cells, enables exceptionally high electrochemical performance, indicated by a power density of $910\,mW\,cm^{-2}$ at 500 °C accomplished for the first time with humidified hydrogen as fuel. This perovskite also demonstrates excellent phase

[*] Dr. W. Zhou, Dr. F. L. Liang
School of Chemical Engineering
The University of Queensland
Brisbane, Queensland 4072 (Australia)
E-mail: wei.zhou@uq.edu.au
Dr. J. Sunarso[+]
Australian Research Council (ARC)
Center of Excellence for Electromaterials Science
Institute for Frontier Materials, Deakin University
221 Burwood Highway, Burwood, Victoria 3125 (Australia)
Prof. M. W. Zhao
School of Physics and State Key Laboratory of Crystal Materials
Shandong University
Jinan 250100, Shandong (People's Republic of China)
Dr. T. Klande, Prof. Dr. A. Feldhoff
Institute of Physical Chemistry and Electrochemistry
Leibniz Universität Hannover
Callinstraße 3A, 30167 Hannover (Germany)
E-mail: armin.feldhoff@pci.uni-hannover.de
[+] Current address:
Department of Chemistry, University of Waterloo
200 University Avenue West, Waterloo
Ontario, N2L 3G1 (Canada)

[**] W.Z. acknowledges the support of the Australian Research Council (ARC). M.Z. thanks the National Basic Research Program of China (grant number 2012CB932302). A.F. and T.K. greatly acknowledge financial support from the Chinese–German Centre for Science (grant number GZ676) and the Deutsche Forschungsgemeinschaft (grant number FE 928/4-1).

Supporting information for this article is available on the WWW under http://dx.doi.org/10.1002/anie.201307305.

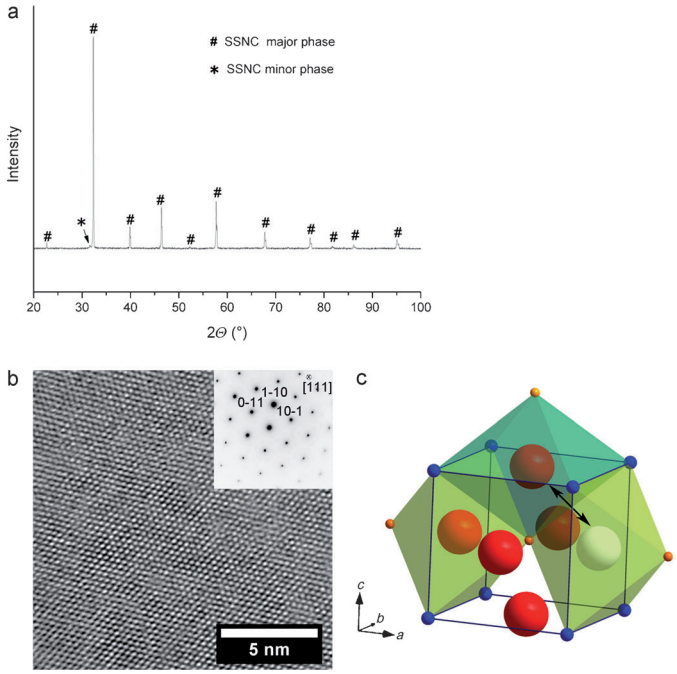

Figure 1. Crystal structure of SSNC. a) Reflections in the X-ray diffraction pattern of SSNC powder are marked by Laue indices. The ⋆ symbol refers to the $(200)_{bm}$ reflection of a brownmillerite by-phase. b) High-resolution transmission electron microscopy analysis of the major phase shows perfect cubic perovskite structure. The inset displays the electron diffraction pattern. c) In the ideal cubic ABO_3 perovskite structure, oxygen occupies octahedral sites and is coordinated by four co-planar A-site cations and two apical B-site cations. A-site cations are blue, B-site cations are orange, and oxygen anions are red (note: The atomic radii are not drawn to scale). The $O(A_{4/12}B_{2/6})$ octahedra share common faces. The white sphere depicts an oxygen vacancy. Oxygen movement from an occupied octahedron to a vacant octahedron, as indicated by a black arrow along the $[10\bar{1}]$ direction, is related to the passing of the octahedron face, which is spanned by two A-site and one B-site cations. This movement is enhanced for the SSNC cathode compared to known standard materials.

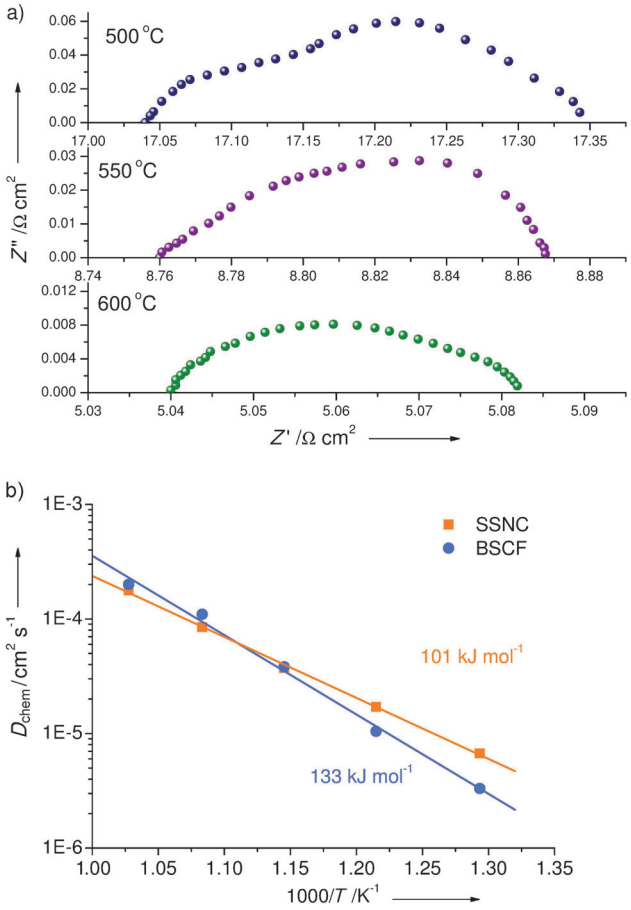

Figure 2. Electrochemical performance of the SSNC cathode. a) Nyquist plots of the SSNC cathode at 500, 550, and 600 °C; b) chemical oxygen bulk diffusion coefficient (D_{chem}) of SSNC and BSCF obtained from the electrical conductivity relaxation (ECR) test. The activation energy of the process is shown.

stability during thermal cycling and long operation, paving the way to performance improvement at low temperatures.

The SSNC powder consisted of a major cubic phase exhibiting primitive lattice in the $Pm\bar{3}m$ space group (#221) with a lattice parameter of $a = 390.4$ pm (Figure 1 a). High-resolution transmission electron microscopy (HRTEM) in conjunction with selected area electron diffraction (SAED) revealed that the majority of grains shows a SSNC structure (Figure 1 b), which is an oxygen-deficient cubic perovskite with oxygen or oxygen vacancies being coordinated by four co-planar A-site cations and two apical B-site cations (Figure 1 c). The existence of Sr, Sc, Nb, and Co in nominal molar ratios is confirmed by energy-dispersive X-ray (EDX) spectra (Figure S1). The minor phase was identified as an ordered brownmillerite phase (see Figure S2a and b in the Supporting Information). The grain boundaries, which may play an important role in exchange processes, were found to be atomically thin without any interphases present (Figure S3a and b).

The ORR activity of the SSNC cathode was probed using a symmetrical cell with an SSNC | $Sm_{0.2}Ce_{0.8}O_{1.9}$ | SSNC configuration. An appropriate amount of SSNC powder in a mixture with solvent and binder was sprayed onto the opposite sides of a $Sm_{0.2}Ce_{0.8}O_{1.9}$ disk and heated to 1000 °C for 2 h to form porous electrodes. X-ray diffraction patterns (Figure S4) ruled out a phase reaction between SSNC and $Sm_{0.2}Ce_{0.8}O_{1.9}$ because no additional phase was formed. Figure 2 a shows Nyquist plots of the SSNC cathode with a thickness of about 10 μm at 500, 550, and 600 °C. The difference between the real axes intercepts on each plot represents the polarization resistance, the values of which are 0.32, 0.11, and 0.04 Ω cm² at 500, 550, and 600 °C, respectively. The use of the area-specific resistance (ASR) term to illustrate the resistance associated with electrode performance is a standard practice in the SOFC field. Lower electrode polarization resistance reflects higher ORR activity. The observed resistance values are extremely low and correspond to the highest ORR activity reported to date. As a reference, we have also prepared and tested a BSCF cathode with a thickness of 10 μm under identical conditions (Figure S5). The ASRs of the BSCF cathode are 0.65, 0.24,

and 0.09 $\Omega\,cm^2$ at 500, 550, and 600 °C, respectively, approximately 100–130 % higher than those of the SSNC cathode. The analogous specific surface area values (obtained from nitrogen sorption measurements) for the SSNC and BSCF cathodes of 0.80 and 0.63 $m^2\,g^{-1}$, respectively, indicate that the improvement of ORR activity is attributed to the higher intrinsic properties of SSNC relative to BSCF.

We sought to clarify the mechanisms behind the excellent performance of the SSNC cathode by performing bulk diffusion coefficient (D_{chem}) measurements using an electrical conductivity relaxation technique (Figure S6). Dense specimens (relative density > 95 %) were used to obtain representative intrinsic properties with minimized impact from microstructures. Figure 2b depicts the Arrhenius plots of D_{chem} for SSNC and BSCF perovskites. Regressed lines were shown to represent the average trend across the considered temperature range. Lower activation energy for D_{chem} for the SSNC [$E_a(D_{chem}) = 101\,kJ\,mol^{-1}$] relative to the BSCF [$E_a(D_{chem}) = 133\,kJ\,mol^{-1}$] translates to distinct performance over the cross-over temperature of about 600 °C. While lower values for D_{chem} are obtained above 600 °C for SSNC, they are enhanced by 64 % and 102 % relative to BSCF at 550 and 500 °C, respectively. Remarkably, such a difference in activation energy magnitude enabled major improvement in the bulk-diffusion properties responsible for the observed excellent ORR activity for SSNC. Moreover, lower electrical conductivities for SSNC with respect to the BSCF (by approximately 20–35 $S\,cm^{-1}$), as shown in Figure S7, suggests that the enhanced ORR activity is not because of the electronic conductivity.

Figure 3a shows the thermal evolution of the area-specific resistance values of the SSNC cathode together with those of other high-performance cathodes prepared under identical conditions. Here, we include a conventional cathode material of $La_{0.6}Sr_{0.4}CoO_{3-\delta}$,[23] a highly active material, for example, BSCF,[20] some recently developed materials such as $SrSc_{0.2}Co_{0.8}O_{3-\delta}$, $SrNb_{0.1}Co_{0.9}O_{3-\delta}$, and $Ba_{0.9}Co_{0.7}Fe_{0.2}Mo_{0.1}O_{3-\delta}$[21,22,24] and layered structure materials such as $PrBaCo_2O_{5+\delta}$[25] and $Ba_2Bi_{0.1}Sc_{0.2}Co_{1.7}O_{6-\delta}$.[26] Between these widely representative perovskite materials, the performance is enhanced in the order of $Ba_{0.9}Co_{0.7}Fe_{0.2}Mo_{0.1}O_{3-\delta} < PrBaCo_2O_{5+\delta} < La_{0.6}Sr_{0.4}CoO_{3-\delta} \approx Ba_2Bi_{0.1}Sc_{0.2}Co_{1.7}O_{6-\delta} < SrSc_{0.2}Co_{0.8}O_{3-\delta} \approx SrNb_{0.1}Co_{0.9}O_{3-\delta} \approx BSCF < SSNC$. The SSNC cathode shows the lowest ASR values among these cathodes with substantial margin over BSCF; it is the only cathode that reaches a target ASR value of 0.15 $\Omega\,cm^2$ below 550 °C.[27] Even at the lowest temperature considered, SSNC has a very low ASR (0.95 $\Omega\,cm^2$ at 450 °C), which is much lower than the ASRs of 2.19 and 2.75 $\Omega\,cm^2$ for BSCF and $SrNb_{0.1}Co_{0.9}O_{3-\delta}$ cathodes, respectively. The exceptionally high ORR activity of the SSNC cathode will enable practical availability of low-temperature SOFCs. The lowest activation energy (E_a) value of ORR for the SSNC cathode (108 $kJ\,mol^{-1}$) is also consistent with its D_{chem} activation energy value, implying the oxygen bulk diffusion as the main contributing factors towards its extraordinary ORR activity. The performance of the SSNC cathode in fuel cells was then investigated on an anode-supported 10 μm $Sm_{0.2}Ce_{0.8}O_{1.9}$ electrolyte. Figure 3b shows a peak power density of 910 $mW\,cm^{-2}$ at 500 °C, the highest value attained to date for an SOFC based on a scalable fuel cell structure.

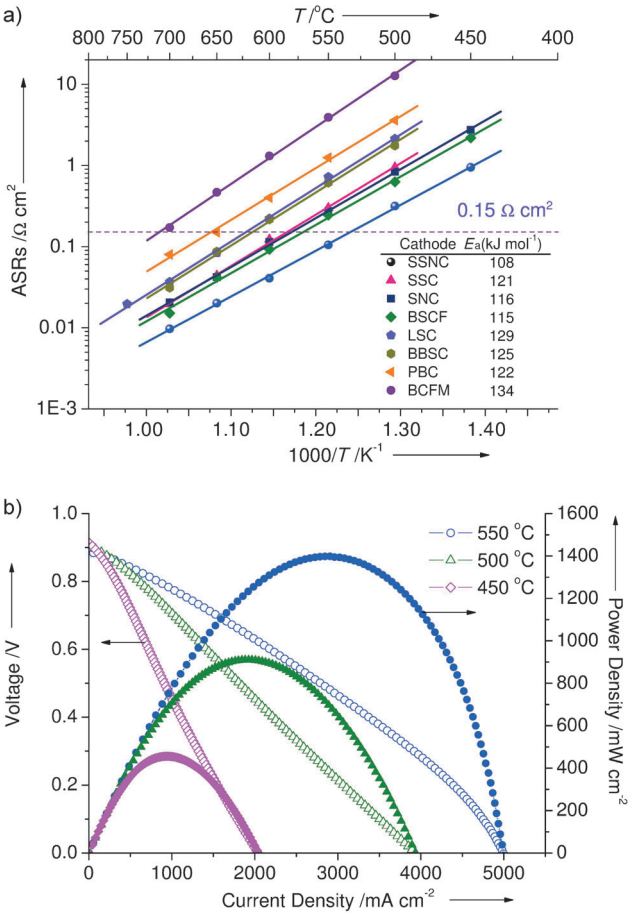

Figure 3. Technical performance. a) Thermal evolution of the area specific resistance (ASR) of the SSNC cathode together with those of other high-performance cathodes prepared under identical conditions to this study. The lowest activation energy (E_a) value of the oxygen reduction reaction (ORR) for each cathode is shown for comparison. The abbreviations of the cathodes are listed in the Supporting Information. b) Cell voltage and power density as functions of current density of a Ni-SDC anode-supported 10 μm SDC electrolyte fuel cell with the 10 μm SSNC cathode operating on hydrogen and air.

In light of understanding the oxygen diffusion in SSNC, first-principles calculations were performed in which dopant (Sc and Nb) atoms were incorporated into a $2 \times 2 \times 2$ supercell of $SrCoO_{3-\delta}$ parent lattices by substituting two Co atoms (Figure 4). Note that in $SrSc_{0.175}Nb_{0.025}Co_{0.8}O_{3-\delta}$, 0.175 moles of Co and 0.025 moles of Co are replaced by Sc and Nb, respectively. The dopant atoms are placed distant from each other for the sake of minimizing the system energy as expected in reality. Therefore, the unlikely condition of two dopant atoms next to one another is ruled out. Given its commonly dominant role in oxygen diffusion, oxygen vacancies (V_O) are the first variable to be studied. Structure considerations show that an oxygen (vacancy) in perovskite is octahedrally coordinated by four co-planar A- and two apical B-site cations, that is, $V_O[A_4B_2]$ or $V_O[A_4B_2]$ octahedral, respectively (see Figure 1c). Ruling out clustering of the minor B-site cations then provides 3 possible types of oxygen

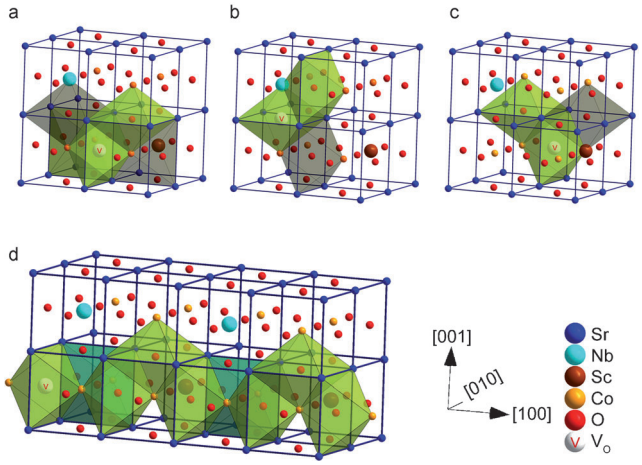

Figure 4. Transport paths for different oxygen vacancy defects in a $SrSc_{0.125}Nb_{0.125}Co_{0.75}O_{3-\delta}$ model. a) V_O [Sr_4Co_2], b) V_O[Sr_4CoNb], c) V_O-[Sr_4CoSc]. The path of V_O[Sr_4Co_2] with the lowest migration barrier is depicted in (d).

vacancies, V_O, with different chemical environments in SSNC, for example, V_O between two adjacent Co atoms, Co-V_O-Co denoted as V_O[Sr_4Co_2] (Figure 4a, the only one in the $SrCoO_3$ parent compound), V_O between Nb and Co atoms, Nb-V_O-Co, denoted as V_O[Sr_4CoNb] (Figure 4b) and V_O between Sc and Co, denoted as V_O[Sr_4CoSc] (Figure 4c). The energies of formation of V_O[Sr_4Co_2], V_O[Sr_4CoNb], and V_O[Sr_4CoSc] are 1.007, 2.164, and 1.906 eV, respectively, which are higher than those of V_O[Sr_4Co_2] in the parent compound $SrCoO_3$ (0.883 eV), thus ruling out enhanced V_O formation as the origin of enhanced transport performance. These values, however, are comparable to those of the V_O in BSCF of about 1.3 eV.[28] From an energetic point of view, the most favorable defect in SSNC is vacancy formation between two cobalt atoms, for example, V_O[Sr_4Co_2]. This may be understood in terms of the higher positive charge of the Sc and Nb dopant atoms compared to Co. Thus, the energy required for vacancy formation in their vicinity is higher.

Turning to another important variable, the possible transport paths of octahedrally coordinated oxygen vacancies, V_O[Sr_4Co_2], V_O[Sr_4CoNb], and V_O[Sr_4CoSc] are depicted in Figure 4a,b and c, respectively. Basically, the migration can be described by a reaction scheme; for example, the migration from a vacancy between two Co atoms into a vacancy (O_o = lattice oxygen) between Nb and Co is shown in Equation (1).

$$\text{Co-V}_o\text{-Co} + \text{Nb-O}_o\text{-Co} \leftrightarrow \text{Co-O}_o\text{-Co} + \text{Nb-V}_o\text{-Co} \quad (1)$$

There are four different paths for V_O[Sr_4Co_2] and two different paths for both V_O[Sr_4CoNb] and V_O[Sr_4CoSc]. Table 1 lists the migration barrier energies associated with all paths. The lowest values correspond to the migration of V_O[Sr_4Co_2] into neighboring V_O[Sr_4Co_2] octahedra with energies of 0.091 eV and 0.185 eV. These values are, in fact, substantially lower than the barrier energies for V_O[Sr_4Co_2] of 0.638 eV in $SrCoO_3$ and 0.42 eV in BSCF,[28] and also lower than those in Sc- or Nb-doped $SrCoO_3$ (Figure S8). It is very likely that the oxygen vacancy travels through these paths, resulting in the migration of oxygen ions along opposite directions (Figure 4d). It may thus be concluded that the excellent transport performance originates from the presence of these favorable transport paths by simultaneous doping of Sc and Nb in SSNC.

We see further potential to improve SSNC-based cathodes if the microstructure is engineered by means of grain size, porosity, and film thickness.[29,30] For practical use, the phase stability at intermediate temperatures has been the main issue for the barium-cobalt-containing perovskites as a result of the formation of hexagonally stacked phases with barium, which is detrimental towards oxygen diffusion.[31–33] We examined the phase stability of barium-free SSNC by performing in situ X-ray diffraction (XRD) between room temperature (30 °C) and 1000 °C. The results (Figure S9) verify the absence of any phase transition, as well as formation of new phase(s), during the heating and cooling processes. The phase stability of SSNC was also tested by annealing the material in air at 600 °C for 100 h (Figure S10).

As a note, ambient air at standard pressure of 101.3 kPa contains carbon dioxide at a partial pressure of circa 30 Pa.[34] Because the formation enthalpy for strontium carbonate is about 30 kJ mole^{-1} lower than that of barium carbonate because of the absence of barium in SSNC, better chemical stability in a carbon-dioxide-containing atmosphere (e.g., air) is expected relative to BSCF.[34,35] Figure S11a shows the long-term performance of the SSNC cathode operated under open circuit voltage (OCV) at 550 and 700 °C. The SSNC cathode maintained constant area specific resistance values of about 0.10 Ω cm^2 (at 550 °C) and 0.01 Ω cm^2 (at 700 °C) during 250 and 125 hour periods, respectively. The cathode also shows high stability under −1000 mA cm^{-2} polarization at 600 °C in air during a 164 hour period (Figure S11b). This highly stable electrochemical performance over a long time period demonstrates that SSNC is applicable as a practical cathode for low-temperature SOFCs. Although a high thermal expansion coefficient of SSNC may potentially impair the compatibility between the SSNC cathode and SDC electrolyte, in all tested samples, no delamination of the cathode was evidenced during the fabrication and thermal cycling (Figure S12).

In conclusion, the results presented herein reveal that very high power density can be achieved in SSNC-derived SOFCs because of the extremely high ORR activity and low activation energy of SSNC. The substantial improvement margin over BSCF represents advancement for the low-temperature SOFC field. Our new composition is also

Table 1: Migration barrier for different transport paths as depicted in Figure 4. The V_O[Sr_4Co_2] octahedra differ in the dopant atom in their immediate vicinity and are marked accordingly.

	Migration barrier [eV]			
	V_O[Sr_4Co_2]-Nb	V_O[Sr_4CoNb]	V_O[Sr_4CoSc]	V_O[Sr_4Co_2]-Sc
V_O[Sr_4Co_2] Figure 4a	0.091	1.260	1.224	0.185
V_O[Sr_4CoNb] Figure 4b		0.104		0.376
V_O[Sr_4CoSc] Figure 4c	0.337		1.172	

promising for further applications requiring mixed ionic–electronic conducting materials, such as oxygen-ion transporting membranes.

Received: August 20, 2013
Revised: October 2, 2013
Published online: November 13, 2013

Keywords: cathode material · electrochemistry · oxygen reduction reaction · perovskite · solid oxide fuel cells

[1] E. P. Murray, T. Tsai, S. A. Barnett, *Nature* **1999**, *400*, 649.
[2] S. Park, J. M. Vohs, R. J. Gorte, *Nature* **2000**, *404*, 265.
[3] Y.-H. Huang, R. I. Dass, Z.-L. Xing, J. B. Goodenough, *Science* **2006**, *312*, 254.
[4] M. Liu, L. Yang, S. Wang, K. Blinn, M. Liu, Z. Liu, Z. Cheng, *Science* **2009**, *326*, 126.
[5] E. D. Wachsman, K. T. Lee, *Science* **2011**, *334*, 935.
[6] E. D. Wachsman, C. A. Marlowe, K. T. Lee, *Energy Environ. Sci.* **2012**, *5*, 5498.
[7] B. C. H. Steele, A. Heinzel, *Nature* **2001**, *414*, 345.
[8] N. Q. Minh, *J. Am. Ceram. Soc.* **1993**, *76*, 563.
[9] M. Tsuchiya, B.-K. Lai, S. Ramanathan, *Nat. Nanotechnol.* **2011**, *6*, 282.
[10] J. Y. Park, H. Yoon, E. D. Wachsman, *J. Am. Ceram. Soc.* **2005**, *88*, 2402.
[11] S. Omar, E. D. Wachsman, J. C. Nino, *Appl. Phys. Lett.* **2007**, *91*, 144106.
[12] D. J. L. Brett, A. Atkinson, N. P. Brandon, S. J. Skinner, *Chem. Soc. Rev.* **2008**, *37*, 1568.
[13] W. Zhou, R. Ran, Z. P. Shao, *J. Power Sources* **2009**, *192*, 231.
[14] S. B. Adler, *Chem. Rev.* **2004**, *104*, 4791.
[15] J. B. Goodenough, *J. Solid State Electrochem.* **2012**, *16*, 2019.
[16] A. J. Jacobson, *Chem. Mater.* **2010**, *22*, 660.
[17] A. Orera, P. R. Slater, *Chem. Mater.* **2010**, *22*, 675.
[18] J. Fleig, *J. Power Sources* **2002**, *105*, 228.
[19] T. Hibino, A. Hasimoto, T. Inoue, J.-I. Tokuno, S.-I. Yoshida, M. Sano, *Science* **2000**, *288*, 2031.
[20] Z. P. Shao, S. M. Haile, *Nature* **2004**, *431*, 170.
[21] W. Zhou, Z. P. Shao, R. Ran, R. Cai, *Electrochem. Commun.* **2008**, *10*, 1647.
[22] W. Zhou, Z. P. Shao, R. Ran, W. Q. Jin, N. P. Xu, *Chem. Commun.* **2008**, 5791.
[23] S. B. Adler, *Solid State Ionics* **1998**, *111*, 125.
[24] S. G. Huang, Q. L. Lu, S. J. Feng, G. Li, C. C. Wang, *Adv. Energy Mater.* **2011**, *1*, 1094.
[25] G. Kim, S. Wang, A. J. Jacobson, L. Reimus, P. Brodersen, C. A. Mims, *J. Mater. Chem.* **2007**, *17*, 2500.
[26] W. Zhou, J. Sunarso, Z. G. Chen, L. Gen, J. Motuzas, J. Zou, G. Wang, A. Julbe, Z. Zhu, *Energy Environ. Sci.* **2011**, *4*, 872.
[27] B. C. H. Steele, *Solid State Ionics* **1996**, *86–88*, 1223.
[28] R. Merkle, Y. A. Mastrikov, E. A. Kotomin, M. M. Kuklja, J. Maier, *J. Electrochem. Soc.* **2011**, *158*, B219.
[29] L. Baqué, A. Caneiro, M. S. Moreno, A. Serquis, *Electrochem. Commun.* **2008**, *10*, 1905.
[30] J. Hayd, L. Dieterle, U. Gontow, D. Gerthsen, E. Ivers-Tiffée, *J. Power Sources* **2011**, *196*, 7263.
[31] K. Efimov, Q. Xu, A. Feldhoff, *Chem. Mater.* **2010**, *22*, 58665875.
[32] P. Müller, H. Störmer, L. Dieterle, C. Niedrig, E. Ivers-Tiffée, D. Gerthsen, *Solid State Ionics* **2012**, *206*, 57.
[33] P. Müller, H. Störmer, M. Meffert, L. Dieterle, C. Niedrig, S. F. Wagner, E. Ivers-Tiffée, D. Gerthsen, *Chem. Mater.* **2013**, *25*, 564.
[34] A. Feldhoff, M. Arnold, J. Martynczuk, T. M. Gesing, H. Wang, *Solid State Sci.* **2008**, *10*, 689.
[35] M. Arnold, H. Wang, A. Feldhoff, *J. Membr. Sci.* **2007**, *293*, 44.